Cent. Eur. J. Phys.
DOI: 10.2478/s11534-013-0280-7

VERSITA

Central European Journal of **Physics**

# Classical spin dynamics of anisotropic Heisenberg dimers

**Research Article**

Laura M. Pérez[1], Omar J. Suarez[2], David Laroze[2,3], Hector L. Mancini[1]*

1 *Departamento de Física y Matemática Aplicada, Universidad de Navarra, Pamplona, 31080, Spain*

2 *Instituto de Alta Investigación, Universidad de Tarapacá, Arica, Casilla 7D, Chile*

3 *Max Planck Institute for Polymer Research, Mainz, D-55021, Germany*

**Received 31 March 2013; accepted 29 June 2013**

**Abstract:** In the present work we study the deterministic spin dynamics of two interacting anisotropic magnetic particles in the presence of an external magnetic field using the Landau-Lifshitz equation. The interaction between particles is through the exchange energy. We study both conservative and dissipative cases. In the first one, we characterize the dynamical behavior of the system by monitoring the Lyapunov exponents and bifurcation diagrams. In particular, we explore the dependence of the largest Lyapunov exponent respect to the magnitude of applied magnetic field and exchange constant. We find that the system presents multiple transitions between regular and chaotic behaviors. We show that the dynamical phases display a very complicated topology of intricately intermingled chaotic and regular regions. In the dissipative case, we calculate the final saturation states as a function of the magnitude of the applied magnetic field, exchange constant as well as the anisotropy constants.

**PACS (2008):** 75.10.Hk, 75.90.+w, 05.45.Ac, 05.45.Pq

**Keywords:** magnetization dynamics • chaos • Lyapunov exponents



## 1. Introduction

Molecular magnetism is becoming increasingly accessible due to the remarkable development of experimental techniques and have found technological applications diverse areas such as quantum computing [1, 2], high-density information storage [3, 4] or magnetic refrigeration [5, 6], just to mention a few. In the last decades, new kinds of molecules with interesting magnetic properties, in which the magnetic moment can be positioned symmetrically in different geometrical configurations, have been synthesized [7]. A simple example is, for instance, unidimensional ring shaped magnetic structures [8–11]. In some temperature regimes, the magnetic properties of these molecules are generally well described by the classical Heisenberg model with small anisotropy corrections [12, 13]. Hence, a detailed study on the dynamical behavior of such magnetic

*E-mail: hmancini@unav.es

systems becomes important for applications.

Standard approaches to study the dynamics of the magnetization reversal are based either on the Landau-Lifshitz [14] or Landau-Lifshitz-Gilbert equations [15], being their time scales the main difference between both approaches for simple systems [15]. Nonlinear problems in magnetism have already been studied in several cases. Recent developments in this field can be found in Refs. [16, 17]. These models have been used in discrete [17–22] and continuous magnetic systems [17, 23–30]. The dynamical behavior of a few magnetic particles interacting through an exchange interaction were studied in Refs. [31–34]. The authors focus on the equilibrium spin-correlation function for different geometrical configurations. The problem of interacting magnetic particles coupled by both short and long-range interaction was analyzed in Refs. [35, 36], concluding that, due to the dipolar interaction, the total magnetization modulus is not a constant, but a fluctuating time dependent function. Recently, a magnetic dimer has been analyzed in a statistical mechanics context, taking into account exchange, dipolar as well as the Dzyaloshinskii-Moriya interactions [37]. Nevertheless, to our knowledge, a parametric study on the dynamical behavior and the corresponding characterization of the chaotic states of two magnetic particles never has been done.

Frequently, maps have been used to describe discrete-time chaotic systems and phase diagrams for these models [38–40], but the problem of building detailed phase diagrams for models ruled by a set of nonlinear differential equations is computationally much harder and has been much less investigated so far. However, diagrams recording complex bifurcations and providing valuable insight for a few of the lowest periods have been obtained in a number of in-depth bifurcation studies using powerful continuation techniques [41–46]. Diagrams recording physically *stable phases* and discriminating simultaneously regions of arbitrarily high periods and regions with chaotic phases, remain essentially unexplored for continuous-time autonomous and non- autonomous dynamical models. Recently, complete phase diagrams have been published for different continuous dynamical models of optically injected semiconductor lasers [47], biophysical [48], and magnetism [49–51]. A review of some of these results can be found in literature Ref. [46], and an standard book of chaos can be found in Ref. [52].

The aim of this paper is to analyze the influence of a constant external magnetic field on a system of two interacting anisotropic magnetic particles. The interaction between the particles is through exchange energy. In particular, we study an applied field in the direction perpendicular to the main anisotropy direction, which is called the easy axis. Also, we focus on the effect of the relative strength interaction between particles. We study both the conservative and dissipative case. Here, we characterize the dynamical behavior by calculating numerically the Lyapunov exponents and bifurcation diagrams. In the dissipative case we calculate the final saturation states as a function of the magnitude of applied magnetic field, the exchange constant, and anisotropy constants. The paper is organized in the following way. In Section 2, the theoretical model is briefly described. In Section 3, the numerical results are provided and discussed. Finally, some conclusions are drawn in Section 4

## 2. Theoretical model

Considering two magnetic particles and assuming that each one can be represented by a magnetic monodomain of magnetization $\mathbf{M}_i$ with $i = (1, 2)$, the temporal evolution of the system can be modeled by the Landau- Lifshitz equation

$$\frac{d\mathbf{M}_i}{dt} = -|\gamma|\mathbf{M}_i \times \mathbf{\Gamma}_i - \frac{\eta|\gamma|}{M_i}\mathbf{M}_i \times (\mathbf{M}_i \times \mathbf{\Gamma}_i), \qquad (1)$$

where, $\gamma$ is the gyromagnetic factor, which is associated with the electron spin and whose numerical value is approximately given by $|\gamma| = |\gamma_e|\,\mu_0 \approx 2.21 \times 10^5\,\mathrm{m\,A^{-1}\,s^{-1}}$. In the above equation, $\eta$ denotes the dimensionless phenomenological damping coefficient which is characteristic for the material and whose typical value is of the order $10^{-4}$ to $10^{-3}$ in garnets, $10^{-2}$ or larger in cobalt, in nickel or in permalloy [17], and $10^{-4}$ in single magnetic molecules [53]. The effective magnetic fields, $\mathbf{\Gamma}_i$, are given by

$$\mathbf{\Gamma}_i = \mathbf{H} + \beta_i\,(\mathbf{M}_i \cdot \hat{\mathbf{n}}_i)\,\hat{\mathbf{n}}_i + J\mathbf{M}_k, \qquad (2)$$

with $(i, k) = 1, 2$ such that $i \neq k$, where $\mathbf{H}$ is the external magnetic field, $\beta_i$ measures the anisotropy along the $\mathbf{n}_i$ axis and $J$ is the exchange coupling constant. Notice that this for this special type of anisotropy, called uniaxial anisotropy, the constants $\beta_i$ can be positive or negative depending on the specific substance and sample shape in use [54]. The exchange constant measures the strength of the interaction between the two particles. Also, $J$ can take positive or negative values depending on the type of interaction; for instance, for $J < 0 (J > 0)$ the coupling will be antiferromagnetic (ferromagnetic). Let us assume that the particles have same magnitude $M_1 = M_2 = M_S$ and the same anisotropy axis $\mathbf{n}_1 = \mathbf{n}_2 = \mathbf{n}$, such that $\mathbf{n} = \hat{\mathbf{z}}$. The external magnetic field $\mathbf{H}$ is assumed to be time-independent and perpendicular to $\mathbf{n}$; hence, without loss of generality, it is fixed along the x-axis: $mathbfH = H_x\hat{x}$.

For zero damping, i.e. $\eta = 0$, Eq. (1) is conservative. In fact, the conservative case has an intrinsic relationship with the Nambu equation [55] governing the dynamics for a triplet of canonical variables with two motion constants. In the case of a single magnetic moment, the triplet of canonical variables are given by $\mathbf{M}$ and the two motion constants are the energy associated to $\Gamma$ and the normalization stationary condition.

It is worth mentioning that in standard materials the macrospin approximation (monodomain particles) is only valid when surface anisotropy effects are not relevant [56]. For larger sizes of particles, non-uniform magnetic states appear, like vortices in cobalt nanodots. In addition, the shape of the nanoparticle plays an important role in the macrospin approximation [57]. In the case of magnetic molecules, this model is only valid in the semiclassical approximation [12, 13], otherwise quantum effects should be considered [58]. Finally, let us remark that due to the nonlinear nature of the problem, analytical solutions can be found only in particular cases; therefore, only numerical studies are possible.

## 3. Numerical results

In order to simplify and speed-up the integration of the equations of motion we use dimensionless units, rewriting Eq. (1) in terms of the magnetization $\mathbf{m}_j = \mathbf{M}_j/M_S$ and time $\tau = t|\gamma|M_s$ [17]. This normalization leads to $|\mathbf{m}_j| = 1$. In order to get a better physical insight into the problem, let us evaluate the scales introduced here. Typical experimental values of $M_S$ are, e.g. for cobalt materials, $M_{S[Co]} \approx 1.42\times10^6$ A/m, for nickel materials $M_{S[Ni]} \approx 4.8\times10^5$ A/m [17]; or for $Mn_{12}$ crystals $M_{S[Mn_{12}]} \approx 4.77\times10^4$ A/m [59]. Leading gyromagnetic frequencies in the Gigahertz range $|\gamma|M_{S[Co]} \approx 308$ HGz, $|\gamma|M_{S[Ni]} \approx 106$ HGz, and $|\gamma|M_{S[Mn_{12}]} \approx 10.5$ HGz, respectively. Hence the time scale ($\tau = 1$) is in the picosecond range, $t_{s[Co]} = 1/(|\gamma|M_{S[Co]}) \approx 3.2$ ps, $t_{s[Ni]} = 1/(|\gamma|M_{S[Ni]}) \approx 9.4$ ps, and $t_{s[Mn_{12}]} = 1/(|\gamma|M_{S[Mn_{12}]}) \approx 95.2$ ps, respectively. Present-day technology is capable of measuring pico- and femto-second processes. Indeed, Beaurepaire et al. [60] were the first to observe the spin dynamics at a time-scale below the picosecond scale in nickel [60]. More recently phenomena at a time-scale less than 100 fs has been observed [61, 62].

To avoid numerical artifacts, it is suitable to solve the corresponding dimensionless Eq. (1) using a Cartesian representation:

$$\begin{aligned}\frac{dm_{x,i}}{d\tau} =& m_{z,i}\left(Jm_{y,k} - \beta_i m_{y,i}\right) - Jm_{y,i}m_{z,k} \\ &+ \eta\left(\left(h_x + Jm_{x,k}\right)m_{y,i}^2 + \left(h_x + Jm_{x,k}\right)m_{z,i}^2 - m_{x,i}\left(Jm_{y,i}m_{y,k} + Jm_{z,i}m_{z,k} + \beta_i m_{z,i}^2\right)\right),\end{aligned} \tag{3}$$

$$\begin{aligned}\frac{dm_{y,i}}{d\tau} =& -h_x m_{z,i} + J\left(m_{x,i}m_{z,k} - m_{x,k}m_{z,i}\right) + \beta_i m_{x,i}m_{z,i} \\ &+ \eta\left(J\left(m_{y,k}\left(m_{x,i}^2 + m_{z,i}^2\right) - m_{y,i}\left(m_{x,i}m_{x,k} + m_{z,i}m_{z,k}\right)\right) - h_x m_{x,i}m_{y,i} - \beta_i m_{y,i}m_{z,i}^2\right),\end{aligned} \tag{4}$$

$$\begin{aligned}\frac{dm_{z,i}}{d\tau} =& h_x m_{y,i} + J\left(m_{y,i}m_{x,k} - m_{x,i}m_{y,k}\right) \\ &+ \eta\left(\beta_i m_{z,i}\left(m_{x,i}^2 + m_{y,i}^2\right) + J\left(m_{z,k}\left(m_{x,i}^2 + m_{y,i}^2\right) - m_{z,i}\left(m_{x,i}m_{x,k} + m_{y,i}m_{y,k}\right)\right) - h_x m_{x,i}m_{z,i}\right),\end{aligned} \tag{5}$$

where $h_x = H_x/M_S$. We note that the second rows of Eqs. (3)-(5) are a consequence of the dissipative term which contain quadratic and cubic nonlinearities. The quadratic terms are produced by the external field, while the cubic coefficients are proportional to the exchange and the anisotropy constants. The conservative part, in each equation, contains quadratic nonlinearities, and linear terms which are generated by the external field. Let us remark that the system has at least two constants of motion (the two individual modulus $|\mathbf{m}_j|$), and when $\eta = 0$, the magnetic energy is also conserved. In the dissipative case, the magnetic energy is not conserved, but it reaches a stationary value after a transient. Given these constrains our systems effective phase space dimension is four. Moreover, we point out that this system has simple homogeneous solutions: $\{\mathbf{m}_1, \mathbf{m}_2\} = \{\pm\hat{x}, \pm\hat{x}\}$, such that

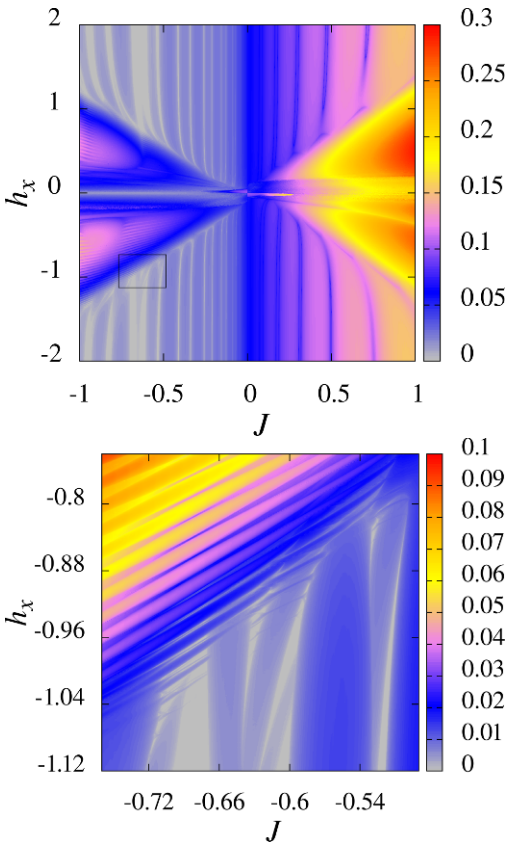


**Figure 1.** (Color online) Phase diagram displaying the largest Lyapunov exponent color coded as a function of the field amplitude $h_x$ and the exchange coupling constant $J$ for two different levels of resolutions. The fixed parameters are $\beta_1 = 0.1$, $\beta_2 = -0.1$ and $\eta = 0$. In both cases the resolution is $10^3 \times 10^3$ Lyapunov exponents.

their stability depends on the control parameters [37].

From the numerical point of view, the integration of Eqs. (3)-(5) has been performed using a standard fourth order Runge-Kutta integration scheme with a fixed time step $d\tau = 0.01$ that ensures a precision of $10^{-8}$ on the magnetization field. In the next subsections we analyze conservative and dissipative regimes respectively.

## 3.1. Conservative regime

In this subsection we first analyze the dynamics of Eqs. (3)-(5) when the dissipation is zero, $\eta = 0$. These equations can have different types of behaviors, from regular to chaotic. One interesting case, in which the system has an analytical solution, is when the anisotropies are null, this means $\beta_1 = \beta_2 = 0$. Indeed, the total magnetization $\mathbf{S} = \mathbf{m}_1 + \mathbf{m}_2$ satisfies

$$\frac{d\mathbf{S}}{d\tau} = -\mathbf{S} \times \mathbf{h}, \tag{6}$$

which is the equation of a single magnetic moment in the presence of an applied field and its solutions is

$$\begin{aligned} \mathbf{S}(\tau) \;=& \begin{pmatrix} S_x(0) \\ 0 \\ 0 \end{pmatrix} + \begin{pmatrix} 0 \\ S_y(0) \\ S_z(0) \end{pmatrix} \cos(h_x \tau) \\ &+ \begin{pmatrix} 0 \\ S_z(0) \\ -S_y(0) \end{pmatrix} \sin(h_x \tau), \end{aligned} \tag{7}$$

where $S_j(0)$ are the initial conditions throughout individual modulus constrains. Also, when the system is anisotropic ($\beta_j \neq 0$) the only possible analytical solutions are when the particles are decoupled $J = 0$. In such case solutions are in the form of Elliptic functions [17].

To characterize the dynamics of Eqs. (3)-(5) we first evaluate the Lyapunov exponents (LEs) [63]. This method consists of quantifying the divergence between two initially close trajectories. The measure of the exponential divergence in phase space is given by the LEs. They are denoted by $\{\lambda_i\}$. Let us recall that one has as many LEs as phase space dimensions within the dynamical system [63]. They can be ordered in descending form, from the largest to the smallest: $\lambda_1 \geqslant \lambda_2 \geqslant ... \geqslant \lambda_N$. The first exponent is the largest Lyapunov exponent (LLE). Here we deal with the non-dissipative regime, and for these types of systems the LEs come in pairs $(\lambda_i, \lambda_{N-i+1})$ such that their sum is equal to zero and at least two LEs are equal to zero. Here, we explore the dependence of the LLE on the different control parameters of the system. One can, e.g., draw two dimensional maps illustrating the magnitude of the LLE as a function of two parameters. This permits to determine the parameter ranges that lead to chaotic dynamics, i.e. LLE positive, and those showing regular (periodic or quasi-periodic) dynamics, LLE zero or negative. In addition, following a technique explained in Ref. [46], we use an iterative zoom resolution process to investigate further the dependence of the dynamics upon very small variations of the system parameters. This technique is generally used for studying dynamical systems that contain chaotic phases with highly complicated and interesting boundary topologies, e.g., curves where networks of stable islands of regular oscillations with ever-increasing periodicity accumulate systematically.

The LEs are calculated for a time span of $\tau = 32768$ after an initial transient time of $\tau = 1024$. The Gram- Schmidt orthogonalization process is performed after every $\delta\tau = 1$.

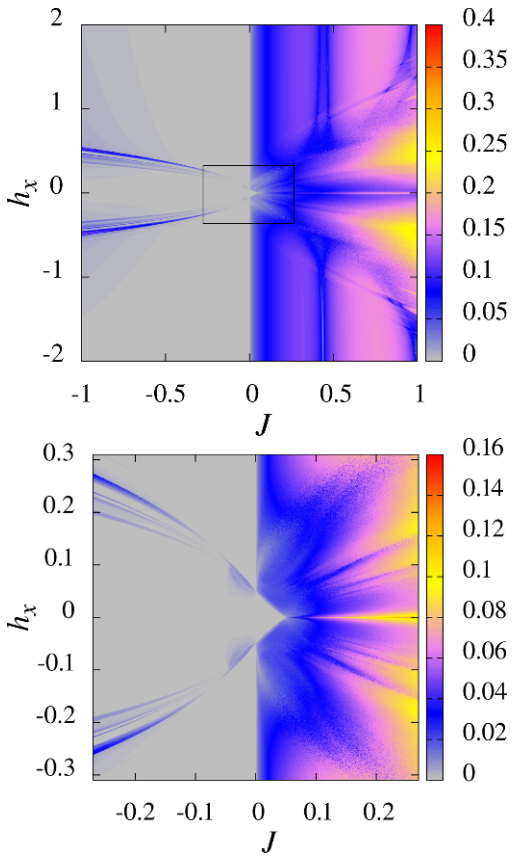


**Figure 2.** (Color online) Phase diagram displaying the largest Lyapunov exponent color coded as a function of the field amplitude $h_x$ and the exchange coupling constant $J$ for two different levels of resolutions. The fixed parameters are $\beta_1 = 0.1$, $\beta_2 = 0.1$ and $\eta = 0$. In both cases the resolution is $10^3 \times 10^3$ Lyapunov exponents.

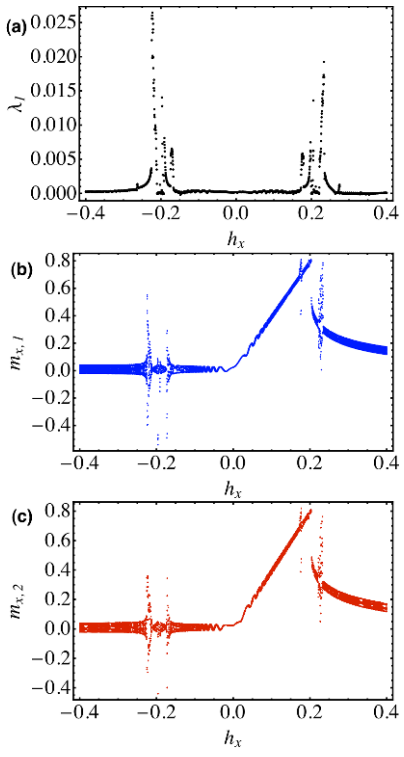


**Figure 3.** LLE and bifurcation diagrams of $m_{x,1}$ and $m_{x,2}$ as a function of the field amplitude $h_x$. The fixed parameters are: $J = -0.2$, $\beta_1 = 0.1$, $\beta_2 = 0.1$ and $\eta = 0$.

The error $E$ in the evaluation of the LEs has been checked by using $E = \sigma(\lambda_1)/\max(\lambda_1)$, where $\sigma(\lambda_1)$ is the standard deviation of the maximum positive LE. In all cases studied here $E$ is of the order of 1%, which is sufficiently small for the purpose of the present analysis.

We note that, there are other methods of quantifying the non-periodic behavior of a dynamical system such as the Fourier spectrum, Poincaré sections, and correlation functions [16, 17, 21]. Also, bifurcation diagrams of magnetization components have been employed in several articles [18, 19, 22].

Figures 1 and 2 show colored code phase diagrams of the LLE as a function of $J$ and $h_x$ for different and equal values of the anisotropy constants, respectively. In both cases their absolute values are the same, such that $\beta_1 = \beta_2 = 0.1$. The left frames show a wide range of the parameters, whereas the right frames show a specific zoom of the corresponding left frame. The zone of the zoom is denoted by a black box. We can observe that the anisotropy energy plays an important role since the diagrams are completely different.

For different anisotropies (Fig. 1) when the exchange coupling constant is positive ($J > 0$) the system is always in chaotic regimes, while for negative values of $J$, multiple transitions between regular and chaotic regimes appear. These transitions can be observed with a best resolution in the right frame of Fig. 1, in which complex patterns in the LLE diagram appear.

Figure 2 shows the LLE as a function of $h_x$ and $J$ at equal anisotropies constants. We can observe that when $J$ is negative the system behaves almost regular except by four plumes located symmetrically respect to $h_x$. For positive values of $J$ the system is in chaotic regimes except for small region when the values of $h_x$. To quantify the dynamics in this region a zoom is shown in the right frame.

In order to investigate in more detail different types of transitions between regular to chaotic behavior we analyze a vertical cross section of Fig. 2 in the range $-0.4 \leqslant h_x \leqslant 0.4$ at $J = -0.2$. The LLE and the bifurcation diagrams of $m_{x,1}$ and $m_{x,2}$ as a function of $h_x$ are presented in Fig. 3(a), Fig. 3(b) and Fig. 3(c). We observe that the system starts in a q-periodic state and makes an abrupt transition to a chaotic behavior. Above

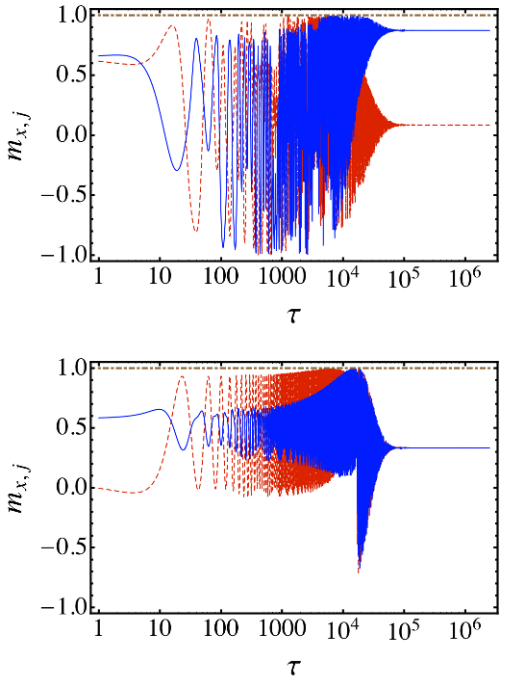


**Figure 4.** x-component of $\mathbf{m}_j$ as a function of time at $\beta_2 = -0.1$ (top) and $\beta_2 = 0.1$ (bottom). The dashed and continues line represent $m_{x,1}$ and $m_{x,2}$, respectively. The dot-dashed line depicts the modulus of $\mathbf{m}_1$. The fixed parameters are $h_x = 0.1$, $J = -0.1$, $\beta_1 = 0.1$ and $\eta = 5 \times 10^{-4}$.

that, alternating regular and chaotic behaviors are found while increasing the parameter $h_x$. For large values of $h_x$ the system becomes regular. Finally, we observe that there is a correspondence between both x-components as shown in our bifurcation diagrams.

## 3.2. Dissipative regime

In this subsection we analyze the case of a dissipative system, $\eta \neq 0$. The values of the damping coefficient in molecular magnetism are small, hence we fix it to $\eta = 5 \times 10^{-4}$. In this case, the common solutions are the stationary ones and reach a constant value after a transient, as shown in Figure 4. This final stationary state is strongly dependent on the parameter values. Indeed, the magnetization of both particles can go to the same value or not, as it is displayed in the left frame of Fig. 4. The type of transient can be regular (like the classical damped harmonic oscillations) or chaotic, depending of the corresponding state of the non- dissipative case. The characteristic decay rate can be elucidated from linear analysis. To estimate the decay rate, we start with an homogenous solution of the system $\mathbf{m}_1 = \mathbf{m}_2 = \hat{x}$ when $h_x > 0$. According to the magnetization conservation condition, we have $m_{x,j} = \sqrt{1 - \left(m_{y,j}^2 + m_{z,j}^2\right)}$. Then for the small deviations the component along the $\hat{x}$ axis can be expressed as:

$$m_{x,j} \simeq 1 - \frac{m_{y,j}^2 + m_{z,j}^2}{2}. \tag{8}$$

Hence, using the standard linear analysis [64] the system reads:

$$\frac{dm_{y,j}}{d\tau} = -\eta(h_x + J)m_{y,j} + (\beta_j - h_x - J)m_{z,j} + \eta J m_{y,k} + J m_{z,k} \tag{9}$$

$$\frac{dm_{z,j}}{d\tau} = (h_x + J)m_{y,j} + \eta(h_x + J - \beta_j)m_{z,j} - J m_{y,k} + \eta J m_{z,k}, \tag{10}$$

where all the $\Theta\left(m_{a,b}^n\right)$ terms of order $n > 2$ have been dismissed. Therefore, the linear system is characterized by the matrix

$$\begin{pmatrix} -(h_x+J)\eta & -h_x - J + \beta_1 & J\eta & J \\ h_x + J & (-h_x - J + \beta_1)\eta & -J & J\eta \\ J\eta & J & -(h_x+J)\eta & -h_x - J + \beta_2 \\ -J & J\eta & h_x + J & (-h_x - J + \beta_2)\eta \end{pmatrix} \tag{11}$$

The eigenvalues of the last matrix, $\sigma$, are obtained by the roots of the secular equation:

$$\sigma^4 + a_3\sigma^3 + a_2\sigma^2 + a_1\sigma^2 + a_0 = 0, \tag{12}$$

where $a_j$, in weakly dissipative regimes, are approximately given by $a_3 = \eta(4(h_x + J) - \Sigma)$, $a_2 = 2h_x^2 + 4J(h_x + J) - \Sigma(h_x + J)$, $a_1 = \eta\left(4h_x^3 + 3h_x^2(4J - \Sigma) + 2h_x\left(4J^2 - 3J\Sigma + \Pi\right) - 2J(J\Sigma - \Pi)\right)$,

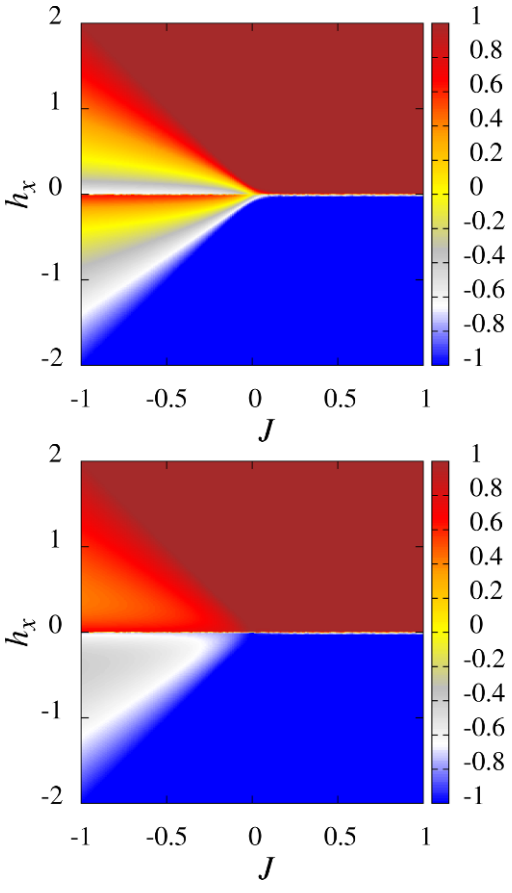


**Figure 5.** (Color online) Phase diagram showing the saturation value of $\tilde{m}_{x1}$ (top) and $\tilde{m}_{x2}$ (bottom) as a function of $h_x$ and $J$. The fixed parameters are: $\beta_1 = 0.1$, $\beta_2 = -0.1$ and$\eta = 5 \times 10^{-4}$.

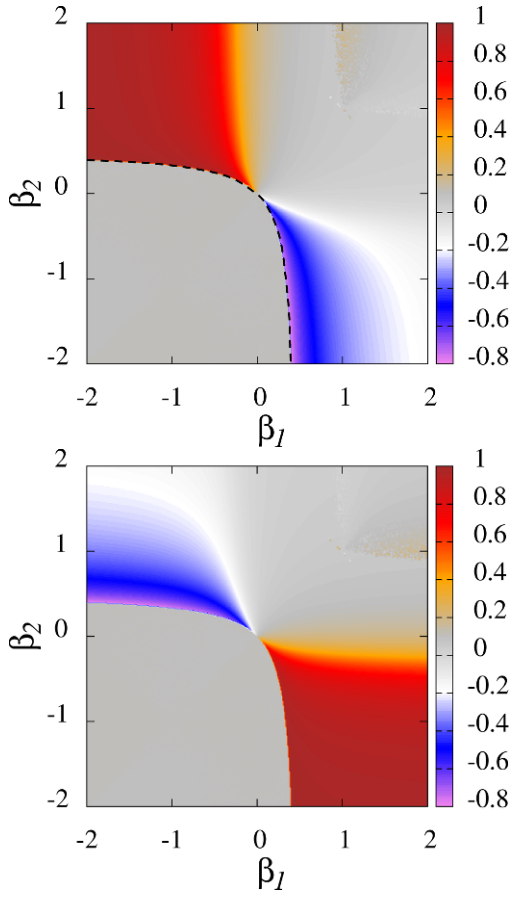


**Figure 6.** (Color online) Phase diagram showing the saturation value of $\tilde{m}_{x1}$ (top) and $\tilde{m}_{x2}$ (bottom) as a function of $\beta_1$ and $\beta_2$. The fixed parameters are: $h_x = 0.1$, $J = -0.1$ and $\eta = 5 \times 10^{-4}$. The dashed line is a fit given by Eq. (13) in the text.

$a_0 = h_x(h_x + 2J)\left(h_x^2 + h_x(2J - \Sigma) - J\Sigma + \Pi\right)$ with $\Sigma = \beta_1 + \beta_2$ and $\Pi = \beta_1\beta_2$. In general, the eigenvalues are complex functions, $\sigma = \sigma_R + \imath\sigma_I = -\mu + \imath\Omega$, such that $\mu$ is the growth factor of the perturbation and $\Omega$ its frequency. Using the inverse of the growth factor one can calculate the characteristic rate decay, denoted here by $\tau_c$. Since, the equation for $\sigma$ is a fourth order one a close form of $\tau_c$ is difficult to obtain analytically and it must be computed numerically. Nevertheless, as a first approximation the characteristic rate decay is $\tau_c \approx 4/[(4(h_x + J) - \Sigma)\,\eta]$. When $J$ $to0$, then $\beta_1 \to \beta_2 \to -|\beta|$ is reduced to $\tau_c \to 2/[(|\beta| + 2h_x)\,\eta]$, which has the same structure that was previously obtained in Ref. [24–29]. In the decoupled system, when $\beta$ is positive $\sigma_R$ becomes positive for $\beta > 2h_x$ producing a linear instability. In our case with $J \neq 0$, when one of the anisotropy constant has different sign the solution always decays if $J > 0$ and if they have the same sign the condition $h_x > -J + \Sigma/4$ guarantees that system does not suffer a linear instability. Let us now to describe how the dynamic-saturation-value of the magnetization, $\tilde{m}_{a,j} = m_{a,j}(\tau \to \infty)$, changes with the control parameters. Figure 5 shows two diagrams of $\tilde{m}_{x,1}$ and $\tilde{m}_{x,2}$ as a function of the external field, $h_x$, and the exchange constant, $J$. Each point in this diagram has been numerically calculated with sufficient integration time to avoid transients ($\tau \gtrsim 10^8$) and with random initial conditions (ICs) on the spheres $|\mathbf{m}|_1 = 1$ and $|\mathbf{m}_2| = 1$ in order to obtain results irrespective of the ICs. We observe that when the coupling constant is positive ($J > 0$), the magnetization of both particles tends to $(\pm)\hat{x}$, depending on the direction of the magnetic field $h_x$. Only in the interface close to $h_x \sim 0$ the magnetization suffers perturbations respect to the x-axis. On the other hand, for $J < 0$, only when $h_x$ is larger than the unity ($|h_x| > 1$), the magnetizations $\mathbf{m}_1$ and $bfm_2$ are oriented along the external field; otherwise, they are oriented in other axes

which depend on the value of $J$ and are not correlated. Furthermore, we analyze the anisotropy effects on dynamic-saturation-values. Figure 6 shows two diagrams of $\tilde{m}_{x,1}$ and $\tilde{m}_{x,2}$ as a function of the anisotropy constants $\beta_1$ and $\beta_2$ at negative values of $J$ and small fields, $h_x = 0.1$. This is the zone of the previous figure when the magnetization of particle one is not correlated with the magnetization of particle two. We observe that in the intermediate region the values of $\tilde{m}_{x,1}$ and $\tilde{m}_{x,2}$ are in anti-phase, such that the anti-symmetry line is the diagonal $\beta_1 = \beta_2$. Moreover, below the curve

$$\beta_2 = \begin{cases} a\tanh\left(b\beta_1 + c\right) & \beta_1 \in (-2.0, 0) \\ \tanh^{-1}\left(\beta_1/a - c\right)/b & \beta_1 \in (0, 0.378) \end{cases} \qquad (13)$$

both $\tilde{m}_{x,1}$ and $\tilde{m}_{x,2}$ are zero when $(a, b, c) = (-0.3845, 1.3477, -0.0442)$, . In fact, in this range the final magnetization states are oriented along the z-axis ($\tilde{m}_{z,1} = \tilde{m}_{z,2} = 1$), which is the anisotropy axis. Also, we can observe that close to $\beta_1 \approx 1$ and $\beta_2 \gtrsim 1$ in the left frame of Fig. 6 there is an isolated cumulus of points in which $\tilde{m}_{x,a} \neq 0$ with small amplitude.

## 4. Final remarks

In this work we studied a classical magnetic dimer in the presence of an external applied field, taking into account anisotropy self-energy and exchange interaction in the Landau-Lifshitz approach. This model can be an interesting tool to describe magnetic molecules in the semi-classical approximation [12, 13], or two interacting magnetic particles in the macrospin approximation when surface energies can be neglected [56]. We have analyzed both, conservative and dissipative regimes. In the conservative case, the system has been mainly characterized through Lyapunov exponents as a function of the parameters and intensive numerical simulations, computing $10^6$ LLE in each two-dimension diagram, have been performed with iterative zooms in the relevant regions. We found that for positive couplings, the system is chaotic in a wide range of magnetic field if the anisotropy constants are equal. This issue is not the same when these constants have the same magnitude but differ in signs, where regular regimes appear for small fields. When the exchange constant is negative, the scenario is completely different. For equal anisotropies the system exhibit regular behaviors for almost all range of magnetic fields, except in four chaotic plume-like regions located in a symmetric way respect to the field. Meanwhile, for different sign of the anisotropy constant multiple transitions between regular to chaotic states are found. These Lyapunov diagrams reveal complex patterns. In the case of dissipative dynamics we have numerically calculated the final stationary solution after a transient. At fixed anisotropy, we have observed that the magnetization of both is oriented along the field when the exchange constant is positive. For negative couplings other orientations are finally reached when $|h_x| < 1$. In this range of fields, for negative exchange when the the anisotropies are varied, there is a region were the magnetic moment of the particles are in anti-phase. Finally, we remark that due to the interaction between particles, different types of synchronizations can be observed. Further research in this direction will be presented in future works.

## Acknowledgements

We thank to T. Corrales (MPI-P) for his critical reading of the manuscript. L.M.P. and H.L.M. acknowledge partial financial MICINN (Spanish Ministry of Science and Technology) under Project FIS2011-24642. O.J.S. acknowledges the financial support from FONDECYT Postdoctoral program fellowship under grant 3130678. D. L. acknowledges partial financial support from Millennium Scientific Initiative, $P10 - 061 - F$, Basal Program Center for Development of Nanoscience and Nanotechnology (CEDENNA) and UTA-project $8750 - 12$.

### References

[1] A. Ardavan, O. Rival, J. J. L. Morton, S. J. Blundell, Phys. Rev. Lett. 98, 057201 (2007)
[2] M. N. Leuenberger, D. Loss, Nature 410, 789 (2001)
[3] M. Mannini et al., Nature Mater. 8, 194 (2009)
[4] L. Bogani, W. Wernsdorfer, Nature Mater. 7, 179 (2008).
[5] M. Manoli et al., Angew. Chem. Int. Ed. 46, 4456 (2007)
[6] G. Karotsis, M. Evangelisti, S. J. Dalgarno, E. K. Brechin. Angew. Chem. Int. Ed. 48, 9928 (2009)
[7] W. Linert, M. Verdaguer (Ed.), Molecular Magnets (Springer, Berlin, 2003)
[8] D. Gatteschi, L. Pardi, A. L. Barra, A. Müller, J. Döring, Nature 354, 463 (1991)
[9] R. Sessoli, D. Gatteschi, A. Caneschi, M. A. Novak, Nature 365, 141 (1993)
[10] D. Gatteschi, A. Caneschi, L. Pardi, R. Sessoli, Science 265, 1054 (1994)
[11] D. Gatteschi, Adv. Mater. 6, 635 (1994)
[12] M. Axenovich, M. Luban, Phys. Rev. B 63, 100407 (2001)
[13] A. Bencini, D. Gatteschi, Electron Paramagnetic Res-

onance of Exchange Coupled Systems (Springer, Berlin, 1990)
[14] L. Landau, E. M. Lifshitz, Phys. Z. Sowjetunion 8, 153 (1935)
[15] T. L. Gilbert, IEEE Trans. Mag. 40, 3443 (2004), and references therein.
[16] P. E. Wigen (Ed.), Nonlinear Phenomena and Chaos in Magnetic Materials (World Scientific, Singapore, 1994)
[17] I. D. Mayergoyz, G. Bertotti, C. Serpico, Nonlinear Magnetization Dynamics in Nanosystems (Elsevier, Dordrech, 2009)
[18] L. F. Alvarez, O. Pla, O. Chubykalo, Phys. Rev. B 61, 11613 (2000)
[19] D. Laroze, L. M. Perez, Phys. B 403, 473 (2008)
[20] P. Diaz, D. Laroze, Int. J. Bif. Chaos 19, 3485 (2009)
[21] D. V. Vagin, P. Polyakov, J. Appl. Phys 105, 033914 (2009)
[22] R. K. Smith, M. Grabowski, R. E. Camley, J. Magn. Magn. Mater. 322, 2127 (2010)
[23] I. V. Barashenkov, M. M. Bogdan, V. I. Korobov, Europhys. Lett. 15, 113 (1991)
[24] M. G. Clerc, S. Coulibaly, D. Laroze, Phys. Rev. E 77, 056209 (2008)
[25] M. G. Clerc, S. Coulibaly, D. Laroze, Int. J. Bif. Chaos 19, 2717 (2009)
[26] M. G. Clerc, S. Coulibaly, D. Laroze, Int. J. Bif. Chaos 19, 3525 (2009)
[27] M. G. Clerc, S. Coulibaly, D. Laroze, Physica D 239, 72 (2010)
[28] M. G. Clerc, S. Coulibaly, D. Laroze, EPL 90, 38005 (2010)
[29] M. G. Clerc, S. Coulibaly, D. Laroze, EPL 97, 30006 (2012)
[30] D. Urzagasti, D. Laroze, M.G. Clerc, S. Coulibaly, H. Pleiner, J. Appl. Phys. 111, 07D111 (2012)
[31] D. Mentrup, J. Schnack, M. Luban, Physica A 272, 153 (1999)
[32] D. V. Efremov, R. A. Klemm, Phys. Rev. B 66, 174427 (2002)
[33] M. Ameduri, R. A. Klemm, Phys. Rev. B 66, 224404 (2002)
[34] R. A. Klemm, M. Luban, Phys. Rev. B 64, 104424 (2001)
[35] D . Laroze, P. Vargas, Phys. B 372, 332 (2006)
[36] D. Laroze, P. Vargas, C. Cortes, G. Gutierrez, J. Magn. Magn. Mater. 320, 1440 (2008)
[37] A. F. Franco, J. M. Martinez, J. L. Déjardin, H. Kachkachi, Phys. Rev. B 84, 134423 (2011)
[38] J. A. C. Gallas, Phys. Rev. Lett. 70, 2714 (1993)
[39] J. A. C. Gallas, Physica A 202, 196 (1994)
[40] B. R. Hunt, J. A. C. Gallas, C. Grebogi, J.A. Yorke, H. Kocak, Physica D 129, 35 (1999)
[41] S. Wieczorek, B. Krauskopf, T.B. Simpson, D. Lenstra, Phys. Rep. 416, 1 (2005)
[42] M. K. Stephen Yeung, S. H. Strogatz, Phys. Rev. E 58, 4421 (1998)
[43] M. K. Stephen Yeung, S. H. Strogatz, Phys. Rev. E 61, 2154 (2000)
[44] M. G. Zimmermann, M. A. Natiello, H. G. Solari, Chaos 11, 500 (2001)
[45] B. Krauskopf, S. Wieczorek, Physica D 173, 97 (2002)
[46] J. A. C. Gallas, Int. J. Bif. Chaos 20, 197 (2010), and references therein.
[47] C. Bonatto and J. A. C. Gallas, Phys. Rev. Lett. 101, 054101 (2008)
[48] J.G Freire, J.A.C. Gallas, Phys. Lett. A 375, 1097 (2011)
[49] D. Laroze, J. Bragard, O. J. Suarez, H. Pleiner, IEEE Trans. Mag. 47, 3032 (2011)
[50] J. Bragard, H. Pleiner, O. J. Suarez, P. Vargas, J. A. C. Gallas, D. Laroze, Phys. Rev. E 84, 037202 (2011)
[51] D. Laroze, D. Becerra-Alonso, J. A. C. Gallas, H. Pleiner, IEEE Trans. Mag. 48, 3567 (2012)
[52] E. Ott, Chaos in Dynamical Systems (Cambridge University Press, Cambridge, 1993)
[53] M. Filipovic, C. Holmqvist, F. Haupt, W. Belzig, arXiv:1211.3611
[54] R. C. O'Handley, Modern Magnetic Materials: Principles and Applications (Wiley-Interscience, New York, 1999)
[55] Y. Nambu, Phys. Rev. D 7, 2405 (1973)
[56] X. Batlle, A. Labarta, J. Phys. D 35, R15 (2002)
[57] P. Landeros, J. Escrig, D. Altbir, D. Laroze, J. d'Albuquerque e Castro, P. Vargas, Phys. Rev. B 65 094435 (2005)
[58] D. V. Efremov, R. A. Klemm Phys. Rev. B 74, 064408 (2006)
[59] J. A. A. J. Perenboom, J. S. Brooks, S. Hill, T. Hathaway, N. S. Dalal, Phys. Rev. B 58, 330 (1998)
[60] E. Beaurepaire, J. C. Merle, A. Daunois, J. Y. Bigot, Phys. Rev. Lett. 76, 4250 (1996)
[61] B. Koopmans, M. van Kampen, J.T. Kohlhepp, W.J.M. de Jonge, Phys. Rev. Lett. 85, 844 (2000)
[62] J. Hohlfeld, E. Matthias, R. Knorren, K.H. Bennemann, Phys. Rev. Lett. 78, 4861 (1997)
[63] A. Wolf, J. B. Swift, H. L. Swinney, J. A. Vastano, Physica D 16, 285 (1985)
[64] M. C. Cross, P. C. Hohenberg, Rev. Modern. Phys. 65, 851 (1993)